SPIN
Vol. 2, No. 4 (2012) 1250017 (11 pages)

DOI: 10.1142/S2010324712500178

World Scientific
www.worldscientific.com

MAGNETO-OPTIC FARADAY EFFECT ON SPIN ANISOTROPIC Co ULTRATHIN FILMS AND POST-NITRIDIZATION ON ZnO(002) CRYSTAL

C. W. SU*, S. C. CHANG and Y. C. CHANG
Department of Electrophysics, National Chiayi University
300 Syuefu Rd Chiayi 60004, Taiwan, R.O.C.
**cwsu@mail.ncyu.edu.tw*

Received 22 December 2012
Accepted 5 February 2013
Published 4 March 2013

Perpendicular magnetic anisotropy in the initial growth of epitaxial in-plane anisotropic Co ultrathin films on the ZnO(002) crystal surface was discovered. The critical thickness of weak spin reorientation transition phenomenon in deposition process from in-plane to out-of-plane magnetic anisotropy is around 2 nm. Ultrathin 1.2 nm Co film was stabilized by post-irradiation of low-energy N ions from the observation of hysteresis loop transforming from an *S*-shape soft magnetic state to a square hard magnetic state. The addition of N affected the magnetic behavior. The time-dependent nitridization process was observed using Auger electron spectroscopy. Magneto-optical Faraday effect measurements were used to observe the magnetic properties of high-transmission Co/ZnO(002) and Co−N/ZnO(002) surface. A strong polar magneto-optic Faraday effect was dominated in the 2.0−4.0 nm Co/ZnO(002) surfaces. From the N^+ implantation that reduces the corresponding coercivity, a hexagonal *c*-axis lattice structure of Co with a preferred perpendicular anisotropy on the ZnO(002) surface may be explained.

Keywords: Nitridization; Auger electron spectroscopy; magneto-optical Faraday effect; ultrathin film; magnetic anisotropy.

1. Introduction

Electronic device applications require precise growth controlling, because the interface structure is usually crucial for further device performances.[1] Recently, magnetic semiconductor (MS) materials have become popular candidates in electronic technological progress; this is because the electric current that carries the initial spin state inside MS materials facilitates the ordering of electron flow. The fluctuating electron spin flow easily loses its memory state without magnetic ordering in the materials. The II−VI magnetic oxide semiconductors, such as diluted magnetic (Zn,Co)O, are among the candidate materials for next-generation spintronic technology.[2−4] Most important issues are concerned that how the inhomogeneous ions incorporated into ZnO possesses excellent n-type or p-type semiconductor property.[5−7] Doping diluted magnetic ions into semiconductors split the spin energy band, resulting in a condition wherein the super exchange interaction between neighboring spins or spin polaron areas induces great enhancement in magnetism. In contrast, doping nonmagnetic ions into ferromagnetic materials may change the original electronic and magnetic states.

This phenomenon has attracted more considerable research attentions.

Recently, magnetic properties of rf-sputtered ZnCoO and ZnCoNO MS films were compared.[8] N-doping in Co:ZnO films exhibits poorly p-type conductivity and paramagnetic. A superparamagnetic behavior in the grown film is observed with increasing the doping content of nitrogen. Doped N atoms are mostly occupying at the O^{2-} anion sites and act as effective N^{3-} acceptors. A charge compensation in ZnCoO films which results from N-doping decreases the free electron carriers.

Thin film ZnO due to the phase possessing high electronic conductivity has been well known. However, a piece of ZnO(002) crystal wafer has high surface resistivity (500 Ω cm to 1000 Ω cm). In this paper, deposition of pure Co on the crystal ZnO (002) may re-examine the relationship between Co and ZnO. Through the deposition of Co ultrathin film the ZnO crystal surface may increase the surface conductivity from insulation state to semiconductor state. Recently, the Co/ZnO series studies is focused because two hcp lattices near interface in which the specific interface Co/O−ZnO or Co/Zn−ZnO problems may generate interesting results with doping p-type anions. In the earlier reports, N ions incorporated with Co/ZnO surface have been confirmed.[9,10] From these studies, the formation of Co−N/ZnO structure is highly possible. The ion energy and sputtering time are the factors to adjust the surface composition of N. The concentration of N is greatly affected by the ion sputtering energy. In this paper, the condition of ion energy is set to 1 keV for observing the series composition and the variation of magnetic signals.

During the deposition of the Co films, magneto-optical effect measurement was initially detected that the magnetic behavior of the 1.2 nm thick Co exhibited only the room temperature longitudinal anisotropy. As the subsequent growth of Co, perpendicular magnetic signal as well as longitudinal magnetic signal was also observed. This result may be attributed to the fact that both Co and ZnO crystalline prefer hexagonal structures (i.e., bulk Co has a hexagonal close-packed (hcp) structure and bulk ZnO has a wurtzite hcp-type structure). A series study on Co nanocolumn embedded in ZnO revealed that magnetization is measured under low temperature (5 K).[11] However, this paper presented that the saturation field of 5 nm Co film expanded to more than 1 T mainly because of superparamagnetic particles, a squareness ($S = M_r/M_s$) smaller than 0.42, and a coercivity of around zero at 300 K. Such features are unsuitable for magnetic application. Therefore, it is necessary to adjust the physical parameters of Co−ZnO to fit room temperature applications. On the other hand, the doping of magnetic oxide semiconductors with nonmagnetic species (e.g., N-doped ZnO or C-doped ZnO), called the d^0 ferromagnetism, has been predicted by first-principle calculations.[12,13] Localized magnetic moment generates magnetic polarons around these nonmagnetic atoms. Thus, doped N ions in ZnO may be possible for generating spontaneous spin polarization and enhancing total magnetization.

$Zn_xCo_{1-x}O$ has superior electronic and magnetic properties, i.e., an intrinsic n-type and diluted ferromagnetic. N-doped ZnO has p-type properties and d^0 ferromagnetism. Thus, merging the interesting issue of reversed electric property and diluted magnetic property from the surface interests us for further study. The variation of magnetic properties such as the squared shape of magnetic hysteresis loop during the plasma nitridization process is especially addressed. Large magneto-optical signals (0.056° in Faraday rotation) with large coercivity (around 53 kA/m) at room temperature and out-of-plane Faraday effect were also observed. Ferromagnetic to paramagnetic transition can be precisely controlled in a short period of time by N plasma sputtering.

2. Experiments

The substrate ZnO(002) single crystal was cleaned by an ion source (Omicron ISE-10) to remove impurities. The cleaning cycle lasted for about 1 h. The sputtering angle was changed to ±20° with respect to the surface normal. The surface was smooth after 15 min off-normal sputtering followed by 15 min plasma irradiation at a low energy of 300 eV. The epitaxial growth of Co ultrathin films was accomplished through evaporation by resistive heating of 99.995% high purity Co filament. Chemical information was obtained by retarding field analyzer-Auger electron spectroscopy (AES) (Omicron spectaLEED/Auger). The surface composition was estimated by the peak-to-peak energy heights in the AES spectra.

An *in situ* magneto-optic Faraday effect (MOFE) technique in the ultrahigh vacuum (UHV) system was designed for the magnetic measurement. The

MOFE was based on the experimental method similar to the surface magneto-optic Kerr effect (SMOKE), which can be used to detect the transmitted magnetic signal of ultrathin films.[14] A linear polarized light passes through a medium in a magnetic field, which generates a Faraday rotation. However, different from the SMOKE, the measured signals of MOFE should consider two contributions: (1) the background Faraday rotation from any dielectric substrates and (2) the main Faraday rotation from magnetic films. However, the study is only focused on the ultrathin film surface and interface within 2−4 nm depth. The magneto-optic signal has been decomposed for the pure MOFE from the ultrathin magnetic films on the surface.

Two configurations in a typical magneto-optic measurement, the longitudinal and polar MOFE, are usually performed. The specimen along the magnetic field with respected to in-plane or out-of-plane can be used to identify the uniaxial magnetic anisotropy. Figure 1 shows the schematic pictures and images captured from the UHV windows. The longitudinal field mode (L-MOFE) and perpendicular field mode (P-MOFE) measurements correspond to Figs. 1(a) and 1(b), respectively. As can be seen, the maximum magnetic field in the UHV system can be achieved at about 255 kA/m under vacuum at 2.7×10^{-8} Pa. The field sweeping rate was about 1.3 kA/(ms). To prevent the degradation or oxidation of the samples, all experiments were *in situ* performed in the same UHV−MOFE chamber without opening to the air.

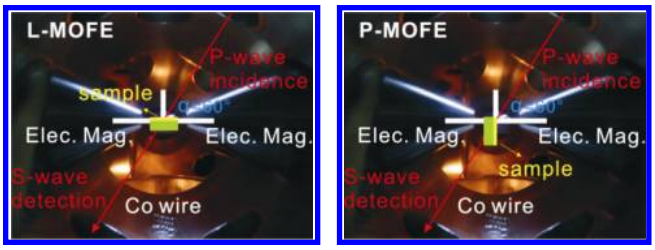

(a) (b)

Fig. 1. MOFE technique performed in a UHV system. The Faraday rotation was measured through the detection of transmitted *s*-polarized light intensity and the rotation of a precise analyzer by the incidence of *p*-polarized light. Figures 1(a) and 1(b) correspond to the longitudinal MOFE (in-plane field) and polar MOFE (out-of-plane field), respectively.

3. Results

3.1. *Preparation of Co/ZnO and Co-N/ZnO film samples and characterization of surface composition and magneto-optic property by MOFE*

Figure 2 shows the schematic of the fabrication procedure of Co/ZnO and Co−N/ZnO samples. The ZnO(002) crystal substrate ($10 \times 10 \times 0.5$ mm^3) was cleaned using a 1 keV direct-current Ar plasma at 2.7×10^{-4} Pa for 1 h. Epitaxial Co molecular beam was deposited at a low rate of 0.57 nm/h for better growth morphology. During the deposition, the contamination of carbon impurities existed but average lower than 5 at.% (fluctuated). The thickness of the ultrathin Co film was estimated by the relative Auger signal ratio. The sample was then transferred to another position for MOFE measurement until the Co became 1.2 nm thick. No hysteresis loop was observed in the epitaxial growth interval until 1.2 nm (data not shown here). Furthermore, the thickness of the 1.2 nm Co/ZnO sample was continuously increased until it reached 1.6 nm. The thickness of the Co sample was successively decreased from 1.6 nm to 1.2 nm by 1 keV N^+ bombardment for about 450 s. In the procedure (3) on the right column of Fig. 2, the schematic diagram means that the ion source of N^+ not only plays a sputtering role but also plays an implantation role. Our recent result shows that surface Co−N layers possibly form interstitial solids or compound layers.[9,10] The former is highly possible in

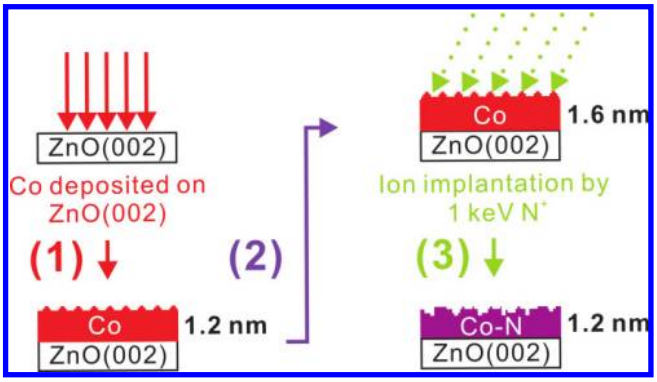

Fig. 2. Sample processing schemes in three steps: (Step 1) Deposition of 1.2 nm Co on ZnO(002) surface by molecular beam epitaxy, (Step 2) Increasing the Co thickness to 1.6 nm and (Step 3) Decreasing the Co thickness and implantation of N^+ into the Co layers to about 1.2 nm by post-sputtering. Under this condition, two samples (1.2 nm Co and 1.2 nm Co− N films) were compared.

most common applications, because the N atom is much smaller than Co. In this study, the N atom was adopted as an impurity species. The impurity atoms fill the interstices among the host atoms.[15]

The surface chemical states of the 1.2 nm Co/ZnO and 1.2 nm Co−N/ZnO samples were characterized by AES. The corresponding spectra (shown at the left side of Fig. 3) were then compared. A clear N KLL-transition signal peak appeared at around 383 eV after an accumulated 1 keV N^+ sputtering for 450 s. Nitrogen sputtering also promoted surface cleanness during processing. Interestingly, 1 keV N^+ sputtering on a bare ZnO (002) surface did not exhibit any N trajectory. The corresponding magnetic hysteresis loop was measured by MOFE after AES measurement. Only the longitudinal hysteresis loops by L-MOFE (in-plane measurements) are shown in Fig. 3. This result indicated that the sample had uniaxial in-plane anisotropy. An S-shape superparamagnetic-like loop was also observed in the 1.2 nm Co/ZnO sample, with a squareness ratio S of 0.42. After the film thickness grew and depleted back to 1.2 nm through N^+ sputtering, the squareness ratio S approached 1 at the same thickness of 1.2 nm N-sputtered Co/ZnO sample. In Sec. 2, we discuss how the N ion incorporated into the surface generates a different effect. Compared with N-free Co/ZnO, the squareness (S) of the Co−N/ZnO sample was around 1 and its coercivity was about 33% larger than that of Co/ZnO. After repeated testing, we also found that the stability of N-sputtered sample can be maintained for more than one week, implying that the post-nitridization of Co/ZnO magnetic surface played a significant role in improving magnetic stability.

3.2. *Observation of time-dependent surface composition via N^+ sputtering and estimation of surface composition versus sputtering time*

We showed that Co/ZnO film can be converted into Co−N/ZnO film through post-N^+ sputtering at the end of Sec. 1. Based on the result, we focused on the experiment on time-dependent Auger intensities that varied with sputtering time. The results are shown in Fig. 4. Chemical data were obtained after each sputtering. During the first 60 min, data were recorded with a step at every 225 s (3 min, 45 s). Except the first 60 min, the interval of sputtering time was lengthened until the end. Focused on the N signal, the variations were clearly divided into three regions as indicated by the abrupt change in curves. These regions were labeled regions I, II and III. The N signal rapidly increased in region I, whereas the Co signal rapidly declined. Numerous N implants appeared in Co in region I. Therefore, the Auger signal of Co decreased with the coverage of N. Given that N signals initially occupied the

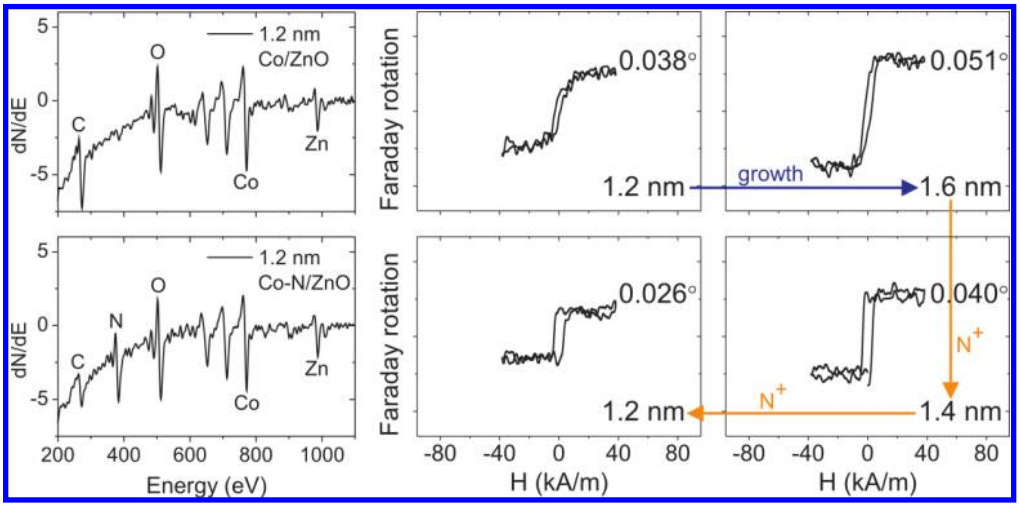

Fig. 3. According to the processing demonstrated in Fig. 2, the hysteresis loops of 1.2 nm Co/ZnO that grows to 1.6 nm Co/ZnO are shown at the top middle to the right figure. Plasma nitridization to 1.4 nm Co−N/ZnO and 1.2 nm Co−N/ZnO are shown at the bottom right to the middle figure. The AES spectra shown at the left column correspond to 1.2 nm Co/ZnO (top) and 1.2 nm Co−N/ZnO (bottom).

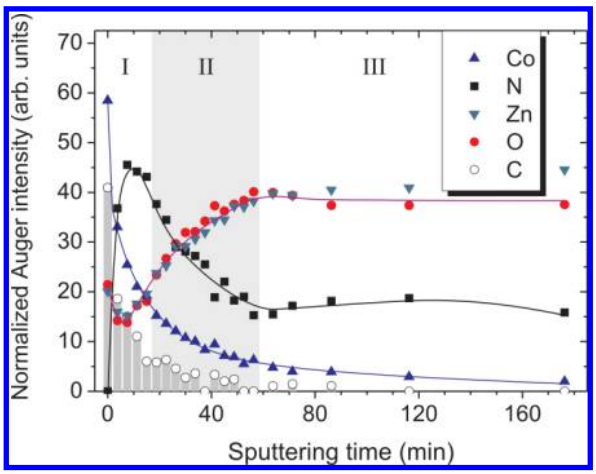

Fig. 4. Variation of Auger electron signal intensity (in arbitrary units) of 1.6 nm Co/ZnO(002) as a function of 1 keV N^+ sputtering time. *y*-axis scale is convenient for visual proportion. From the variations of N signal, the curves were divided into three regions: I: initial implantation of N into Co/ZnO, II: parallel depletion of Co and N by N^+ sputtering and the resulting thinning of the Co layer, and III: diffusion of Co−N into the top surface layer of ZnO.

entire surface, both substrate signals from Zn and O in region I relatively decreased. At 20 min, the Co signal exponentially decreased. Zn and O signals also revealed that the top of the Co film began to deplete away from the surface. An interesting behavior in Sec. 2 showed that the N signal followed the same exponential decay as that of Co. The sputtering effect of N occurred in the region with the same depleting rate as Co. Following this trend, the composition ratio of N and Co was around 2.5. All signals were saturated until most of the Co was depleted from the surface.

Auger depth profiling is a well-known surface-sensitive technique that yields compositional information. Exposing the surface under an ion beam, which leads to the sputtering of surface atoms, is an efficient way of simultaneously observing variations in surface composition. However, this technique sometimes uses Ar plasma to prevent chemical destruction on the surface. We have recently studied the sputtering species that exchanges Ar with N, and have obtained a series of results for the dependence of ion energy and sputtering time.[9] Region II in Fig. 4 indicates that the relative composition ratio of N and Co keeps approximately constant. The thickness of Co−N with sputtering time was depleted successively without changing the composition of N inside Co−N layers. Surface information in regions I and III remained lacking, i.e., the implantation in the Co layers (region I) and the assumed diffusion layer in the substrate ZnO surface (region III). We emphasized earlier that the implantation of N^+ into surface layers is the key factor that affects the corresponding magnetic properties in this study. Considering the nitridization, thinning effect, and diffused layers at the substrate surface in the N_+ sputtering process, the empirical composition formula that focuses on Co and N constituents by combining surface adsorption and the predicted time-scaling power law can be expressed as[16]:

$$\left.\begin{aligned} C_{\mathrm{N}} &= \mathrm{C}^0_{\mathrm{N}} \times (1 - \mathrm{e}^{-bt}) + k - m \times t^n \\ C_{Co} &= \mathrm{C}^0_{\mathrm{Co}} \times \mathrm{e}^{-bt} + k - m \times t^n \end{aligned}\right\} \quad (1)$$

where t is the sputtering time. Assuming that the compositional variations in N and Co are more dominant than the ZnO surface layers, then the total percentage sums for N and Co are both equal to 1; thus, Eq. (1) results. The composition of Co−N results in CoN_3.

Equation (1) fits well except for the adsorption of N into the surface layers of Co in region I and saturation in region II after shadow region labeling at 7.5 min (see Fig. 5). This indicated that a buried diffusion layer of N−Co in the ZnO surface existed in region III after approximately 40 min. After a long sputtering process, the N trajectory ultimately resided on the surface. A different result that no N trajectory observed on bare ZnO(002) surface was compared with the same condition but without Co layers covered.

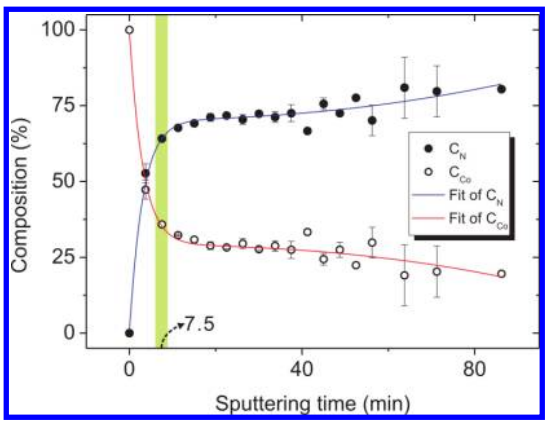

Fig. 5. Relative time-dependent surface compositions of Co and N were calculated. The compositions were estimated and fitted from the t^n scaling law.[16]

3.3. *Observation of growth of Co and time-dependent MOFE via 1 keV N^+ sputtering*

From the observation of relative surface composition via sputtering time in Sec. 2, N was clearly incorporated into the surface layers of the top Co/ZnO. We alternatively observed that the magnetic properties of N^+ irradiated Co/ZnO varied with sputtering time. The longitudinal (L-) and polar (P-) MOFE hysteresis loops of a 4 nm Co/ZnO sample were observed by the time-dependent nitridization effect (see Fig. 6). The 4 nm Co/ZnO(002) film grew via a four-stage deposition process, in which the growth rate was 1 nm/h with an 8 h break. The corresponding L-MOFE and P-MOFE hysteresis were taken at loop 1 (as-deposited), loop 2 (after 113 s N^+ sputtering) and loop 3 (after 225 s N^+ sputtering), as shown in Figs. 6(a) and 6(b), respectively. No hysteresis behavior was observed during long N^+ sputtering because the successive sputtering yielded a nonmagnetic N-rich Co−N phase. According to the studies of Fe or CoFe sputtered films, they have been magnetically softened by controlled N-doping during sputter depositions.[17,18] A ferromagnetic−paramagnetic transition occurred. A reduction of Hc in the CoFe series film has also been observed with a 60% reduction of mean grain size. According to the previous time-dependent composition curve shown in Fig. 4, the observations of MOFE within the 7 min locating at region I revealed diluted N doping. In that period of time, N ions continuously incorporated with top Co layers to form Co−N; hence,

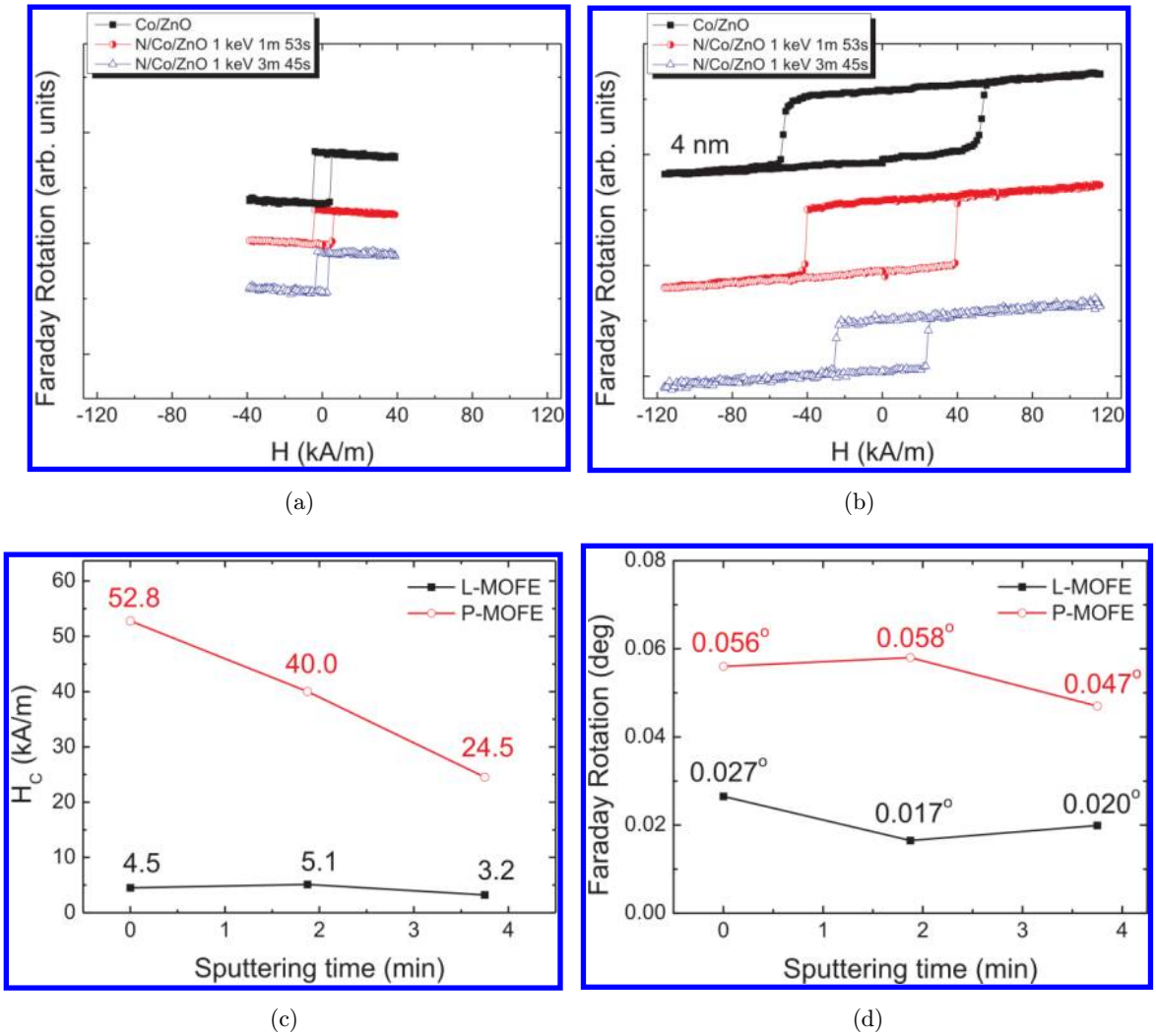

Fig. 6. Magnetic properties L-MOFE (a) and P-MOFE (b) modes were observed by post-N^+ sputtering for the 4 nm Co/ZnO film. Variation of coercivity (c) and Faraday rotation (d) with sputtering time were measured from the hysteresis loops (a) and (b) herein.

the ferromagnetic phase of Co-rich Co_xN was dominated. No hysteresis loop can be observed across the N peak. Figure 6 presents the variations in large perpendicular MOFE. In the as-deposited 4 nm Co/ZnO sample, the coercivity (Hc) was estimated about 4.5 kA/m in the longitudinal mode, whereas the corresponding Hc in polar mode was 10 times larger (about 53 kA/m) as seen in Fig. 6(c). Interestingly, Hc in the polar mode obviously declined larger than Hc in the longitudinal mode. All longitudinal coercivities were maintained at only around 4.0 ± 0.8 kA/m, whereas the polar Hc obviously declined at a step (around 12 kA/m to 16 kA/m), as shown after each sputtering in Fig. 6(c). Moreover, perpendicular anisotropy weakened with increasing nonmagnetic Co−N phase after more N ions were doped into the out-of-plane surface Co layers. In-plane anisotropic Co layers close to the ZnO surface may leave. Therefore, the corresponding *in situ* P-MOFE and L-MOFE loops during the growth process of Co in the same UHV−MOFE chamber are further checked as shown in Fig. 7. In the thickness-dependent MOFE measurement, the hysteresis loops demonstrated that magnetic anisotropy gradually reoriented toward from in-plane to out-of-plane with increasing Co thickness up to 2.3 nm. Due to the low Hc locating at the in-plane direction, the macroscopic magnetic anisotropy of Co/ZnO is in-plane. Generally, the magnetization should be weakened from easy axis to hard axis.[19] However, in our case, the out-of-plane signal is larger than in-plane signal. The MOFE signal is proportional to the magnetization of the film. Thus, the easy axis canted toward the out-of-plane direction became visible as the Co grew thicker than 2 nm. Saturated loops simultaneously occurred at both P- and L-directions after 2 nm, which meant that the magnetic easy axis may be canted with respect to the surface normal. The M-plane (parallel to *a*-axis) lattice mismatch between Co and ZnO bulk lattice (about 22.8%) was quite large, indicating that the strain interaction of the grown magnetic nanograins with the interface was larger. A clear surface effect in which only longitudinal MOFE signals were observed, also agreed with the observation in Fig. 7 for Co less than 2 nm thick. Large grains eased the interface strain as Co grew, and a topmost bulk-like hcp structure with a *c*-axis easy axis was formed. In addition, the bulk-like behavior of Co (over 2 nm thick) indicated that the *c*-axis magnetocrystalline anisotropy began to dominate in the top Co structure. Generally, surface roughness lower than 1 nm is not easy to identify with atomic force microscope (AFM). We have observed the initial ZnO(002) surface by *ex situ* AFM and obtained nothing about roughness information. From the recent study on the surface roughness of the deposited Co/sputtered−ZnO surface, critical thickness of Co determined by AES and MOFE just matches around 2 nm.[20] Thicker than 2 nm as shown in the report, the behavior of Faraday intensity returns to an approximately linear growth with bulk-like Co thickness. The result implies that the surface roughness is strongly related to the fluctuation of optical signals.

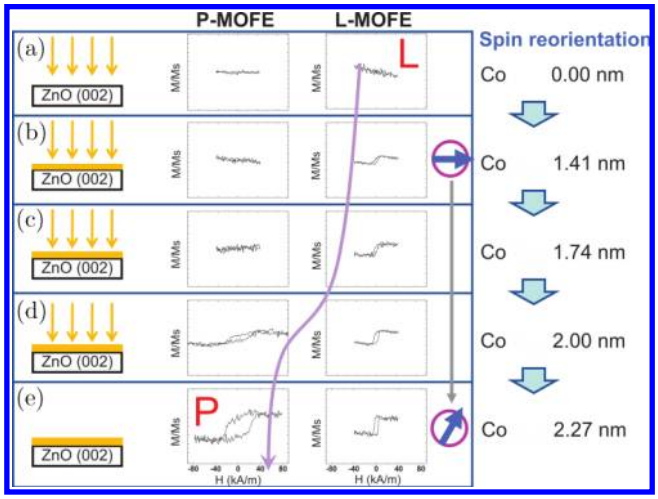

Fig. 7. P-MOFE and L-MOFE hysteresis loops observed in the growth of Co. Variations of thickness from 0 nm to 2.27 nm are labeled from (a) to (e), respectively. The clear MOFE loop was detected at about 1.4 nm. L-MOFE domination gradually transited to P-MOFE domination as thickness increased.

3.4. *Surface condition observed through angle-dependent transmitted interference method*

Figure 8 demonstrates the optical mapping profile of received s-polarized intensity versus the angle of incidence. Generally, absorption and reflectance are relevant factors in most optical techniques, such as spectroscopic ellipsometry.[21−23] Intense transmission carries too much background intensity for a high transparency crystal in most optical design. It is not easy to analyze the structural-related optical information without filter. To avoid the effect produced by ordinary and extraordinary beams, linear polarized prisms in the MOFE technique was used.

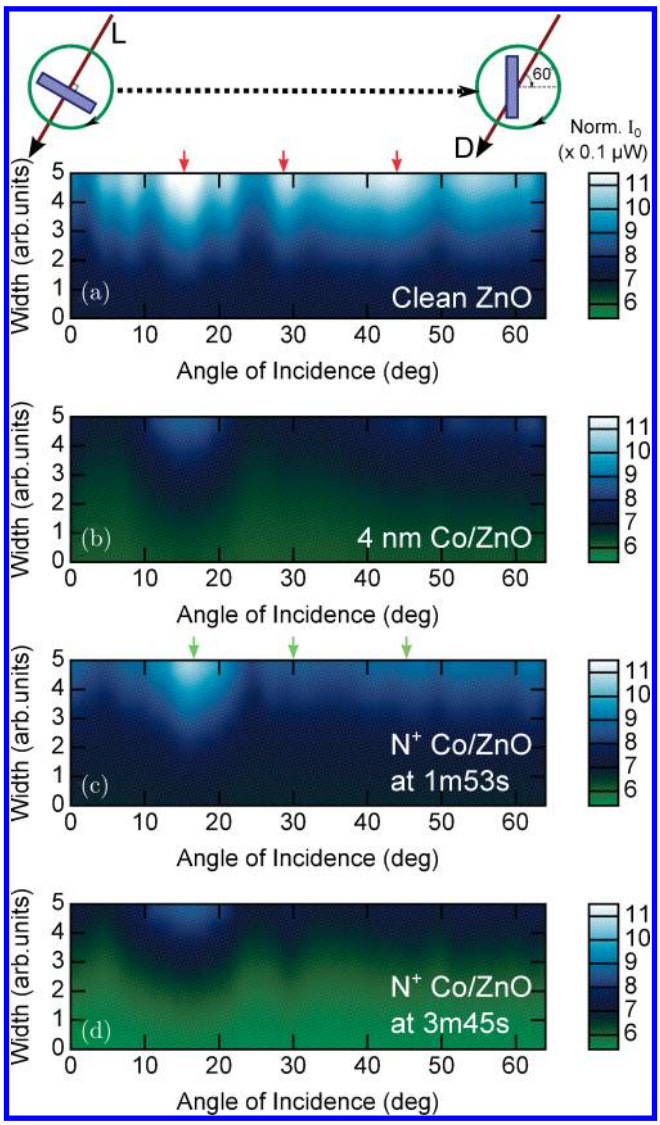

Fig. 8. Interference mapping profile generated from the received *s*-polarized intensity in MOFE measurement was observed by the variation of angle of incidence in the polar plane. Label L and D on the figure means laser and detector. All samples were scanned from 0° (incident direction parallel to surface normal) to around 66° (near P-MOFE side). The vertical *y*-axis scale simulated by SPYVIEW code is arbitrary. The normalized gradient color in the *z*-axis bar reveals the received optical intensity I_0. All optical spot images have been regenerated by a low-pass filter. Four samples are compared: (a) clean ZnO(002), (b) 4 nm Co as-deposited, (c) N^+ sputtered Co/ZnO at 113 s and (d) N^+ sputtered Co/ZnO at 225 s.

Without the use of polarizer, a modulated interference fringes ensemble may be obtained.[24] Hence, the sensitive weak s-polarized intensity in a p-polarized incidence has a great advantage in the examination of surface or interface structure.[25]

The cross polarizer blocks most of the background intensity from the p-polarizer. The minimum intensity (I_0) was measured at zero magnetic field. Figure 8 record I_0 versus the angle of incidence (the angle is with respect to the surface normal) from normal incidence (0°) to the P-MOFE point (∼ 60°). Over 60 s-polarized optical intensity data per sample with 1 degree resolution were measured. A signal to image code (SPYVIEW program) is used to transform the optical intensity to the optical mapping.[26] Interestingly, the interference-like oscillation behavior in this uniaxial ZnO(0001) crystal system was observed. The MOFE configuration as a laser interferometer is used to observe the optical interference fringes. Surface flatness is determined by measuring from the fringe shift.[27] Four different specimen conditions in Fig. 6 were compared by this method. It is noticed that the normalized color scale corresponds to the optical intensity through an optical power meter. The main peak intensity around 15° was observed in Figs. 8(a) to 8(d). The angle depends on the crystal thickness. In Fig. 8(b), covering a 4 nm Co film on ZnO surface absorbed the overall optical intensity and reduced the multiple scattering between the interfaces. Thus, the fluctuation of optical signals in Fig. 8(b) is very low. Deposition of Co leads to the absorbed layer blocked most transmission rays from the reduced background intensity. The optical signal in the first sputtering at 113 s [see Fig. 8(c)] exhibits high transmission intensity with diffuse signals as a clean ZnO sample. The more the bright interference spots, the smoother the surface. The bright spot region therefore reflects the surface condition within optical resolution. Successive sputtering at the second sputtering time 225 s may cause the roughness which degrades the overall optical signals [spot background intensity in Fig. 8(d) becomes much lower than that in Figs. 8(b) and 8(c)]. Further N^+ sputtering induces simultaneously surface implantation and depletion. The rough surface should be expected. The surface treatment may directly alter the surface roughness that is related to our recent observation by optical method. Focused on the Fig. 8(c), the peak positions around 15°, 29° and 44° after the 113 s N^+ sputtering are all shifting about 2° to the right from the comparison of bright spots in Figs. 8(a) and 8(b). The shift of the spot reflects the macroscopic variation of surface morphology altered by N^+ ions or from the optical properties of

the Co−N layers. The formation of Co−N in this treatment corresponds to region I of time-dependent N composition curve in Fig. 4. The inference makes sense because the N^+ depletion has not yet begun. The drop of the optical interference intensity mapping and divergence of bright regions in Fig. 8(d) (sputtering time at 225 s) was observed. It is noticed that the bright region between 10°−20° and 40°−60° is very similar to the positions in Fig. 8(b). Especially, the sharp peak at around 30° is appeared as same as the result in Fig. 8(a). Combined these characteristic points the surface may be gradually back to initial rough condition. Successive long-time N^+ sputtering not only depletes the covered region of Co but causes the possibility of exposure of clean ZnO surface.

4. Discussions

Reduction of out-of-plane anisotropy can be directly verified and proven if more N ions depleted or incorporated with the top Co layers. Perpendicular spins may be gradually destroyed and returned to in-plane anisotropy at an initial growth of around 1.4 nm. Figure 6(d) recorded the longitudinal Faraday rotation angle and perpendicular Faraday rotation angle for the as-deposited Co/ZnO at 0.027° and 0.056°, respectively. The magnetic easy axis of the film according to trigonometric operation favored 25.7° with respect to the surface normal. Moreover, as seen in Fig. 6(d), P-MOFE signal increased, whereas the L-MOFE signal decreased after 113 s (1 min 53 s) of N^+ sputtering because the implantation effect of N was dominant (compared with region I in Fig. 4). The time point of N^+ sputtering at 225 s (3 min 45 s) revealed that a depleting effect was dominant because both P-MOFE and L-MOFE rotation angles were reduced. The surface anisotropy at the thickness, with an initial growth of in-plane Co anisotropy, also returned. Interestingly, the 4 nm Co case can be classified as a thick polycrystalline film in an ultrathin regime. Shape anisotropy is dominant when the magnetization of magnetic particles is axial symmetric and ellipsoidal; moreover, the energy depends on the direction of magnetization. The magnetization switches direction at the critical magnetic field, i.e., the coercive field Hc. Shape anisotropic energy K_{us} or crystalline anisotropy constant K_1 can be simply expressed as $K = 1/2M{\cdot}Hc$, and K is always positive for Co regardless of whether or not K_{us} or K_1 is used. The magnetic energy reaches its minimum for stability at the crystal axis, which has a relatively large coercive field. In this case, Co/ZnO(002) and its related Co−N/ZnO(002) system favored perpendicular configuration because of the native hcp-type structure of bulk Co and ZnO. Likewise, the easy axis of bulk Co was located along the [0001] *c*-axis. The thick film showed more anisotropic energy contributed in perpendicular term compared with the strong longitudinal anisotropy of the thin Co/ZnO sample in Fig. 3. When the top layer was depleted by sputtering, the magnetic thickness was decreased and returned back to that of the initial grown film with in-plane configuration. The effect is exactly the opposite of the result for different substrates recorded in a previous work.[28] Although the corresponding magnetic property of the thin film structure with the same thickness may be altered by different growth environments in terms of deposition rate, vacuum level and substrate orientation, among others, our result provides a processing tread for further reference.

Based on the results, the MOFE signal dominates in the longitudinal field mode during the initial growth of Co. The observed in-plane anisotropy may be attributed to the segregation effect generated during a long-time deposition processing period. The pseudomorphic growth of fine Co particles on the ZnO may have in-plane interface anisotropy, whereas particles grown further may enhance super exchange coupling to reveal bulk-like, out-of-plane anisotropy. According to a recent study about defects on the ZnO(0001) polar surface observed via scanning tunneling microscope (STM) technique, O-terminated hexagonal cavities and Zn-terminated triangular Islands coexist due to the balance of electrostatic energy on the surface.[29] This can be attributed to the surface structure that may favor the easy axis parallel to the plane, or an additional in-plane anisotropic contribution of CoO that provides possibilities in the total magnetocrystalline anisotropy.[30] Further deposition of Co eases the effect, resulting in strong out-of-plane anisotropy. This inference about defect depth and interaction length between defect pits on the surface plane, compared with our observation of the spin reorientation at around 2 nm, is completely in accordance with the STM and AES observations.[20,29] The squared hysteresis loop irradiated by N^+ ions enhances the application potential. Generally, the

flux available for magnetic recording with sharp transition is characterized by squareness. This effect is responsible for developing magnetic memory devices.[31] According to the composition experiment via the sputtering time of N^+, the Co layer was rapidly depleted, and N species dramatically grew within the initial 450 s. Thus, the electronic properties of the material still require further examination. Moreover, the film thickness can be precisely controlled through this technique by focusing the N^+ sputtering. In effect, controlling the fine thickness by post-N^+ sputtering has become more effective and easier.

5. Conclusion

In this study, 1 keV dc N^+ sputtering with Co/ZnO (002) surface generates surface nitridation. N^+ plays two roles in Co/ZnO: (1) implantation of N into the Co layers and (2) depletion of Co from the ZnO surface. Therefore, except processing the Co−N films has to consider nitridation, the thickness depletion is also the key factor. The core magnetic properties in this period exhibit application potential. As thickness of Co grows thicker than 2 nm, the magnetic anisotropy of hcp crystalline Co/ZnO favors the out-of-plane orientation. A large reduction in coercivity about 0.126 kA/(m s) was observed in the 4 nm thick Co/ZnO film by the polar MOFE. Observation of relative surface roughness through related optical interference image is convinced with AES and MOFE measurement by optical mapping method. Followed by the post-short-period N^+ implantation process, hard magnetic state to soft magnetic state can be precisely controlled. For industry, this processing is convenient and efficient. Besides, the ion depletion process can also be flexibly used to control media patterning in progressive perpendicular recording technology.

Acknowledgments

This project was supported by the National Science Council of Taiwan, the Republic of China, and National Chiayi University (Grant Numbers: NSC 98-2112-M-415-003-MY3 and 101-2112-M-415-004).

References

1. H. L. Meyerheim, C. Tusche, A. Ernst, S. Ostanin, I. V. Maznichenko, K. Mohseni, N. Jedrecy, J. Zegenhagen, J. Roy, I. Mertig and J. Kirschner, *Phys. Rev. Lett.* **102**, 156102 (2009).
2. Y. B. Zhang and S. Li, *Appl. Phys. Lett.* **93**, 042511 (2008).
3. F. Hu, Q. Liu, Z. Sun, T. Yao, Z. Pan, Y. Li, J. He, B. He, Z. Xie, W. Yan and S. Wei, *J. Appl. Phys.* **109**, 103705 (2011).
4. S.-S. Yan, C. Ren, X. Wang, Y. Xin and Z. X. Zhou, L. M. Mei, M. J. Ren, Y. X. Chen and Y. H. Liu, H. Garmestani, *Appl. Phys. Lett.* **84**, 2376 (2004).
5. C. H. Park and D. J. Chadi, *Phys. Rev. Lett.* **94**, 127204 (2005).
6. S. Zhou, K. Potzger, J. von Borany, R. Grötzschel, W. Skorupa, M. Helm and J. Fassbender, *Phys. Rev. B* **77**, 035209 (2008).
7. T. M. Barnes, K. Olson and C. A. Wolden, *Appl. Phys. Lett.* **86**, 112112 (2005).
8. Y.-H. Lee, J. C. Lee and C.-W. Su, *IEEE Trans. Magn.* **46**, 1565 (2010).
9. C. W. Su, M. S. Huang, Y. C. Chang, T. H. Tsai, Y. H. Lee and J. C. Lee, *J. Appl. Phys.* **105**, 033509 (2009).
10. C.-W. Su, Y.-C. Chang, T.-H. Tsai, S.-C. Chang and M.-S. Huang, *Thin Solid Films* **519**, 3739 (2011).
11. N. Jedrecy, H. J. von Bardeleben and D. Demaille, *Phys. Rev. B* **80**, 205204 (2009).
12. L. Shen, R. Q. Wu, H. Pan, G. W. Peng, M. Yang, Z. D. Sha and Y. P. Feng, *Phys. Rev. B* **78**, 073306 (2008).
13. K. Yang, R. Wu, L. Shen, Y. Ping Feng, Y. Dai and B. Huang, *Phys. Rev. B* **81**, 125211 (2010).
14. Z. Q. Qiu and S. D. Bader, *Rev. Sci. Instrum.* **71**, 1243 (2000).
15. W. D. Callister, *Material Science and Engineering: An Introduction*, 7th edn. (Wiley, New York, 2007).
16. Y. Wang, S. F. Yoon, C. Y. Ngo, C. Z. Tong and C. Y. Liu, *J. Appl. Phys.* **106**, 024301 (2009).
17. M. Vopsaroiu, M. Georgieva, P. J. Grundy, G. Vallejo Fernandez, S. Manzoor, M. J. Thwaites, K. O'Grady, *J. Appl. Phys.* **97**, 10N303 (2005).
18. M. T. Georgieva, N. D. Telling and P. J. Grundy, *Mater. Sci. Eng. B* **126**, 287 (2006).
19. H. P. Oepen, A. Berger, C. M. Schneider, T. Reul and J. Kirschner, *J. Magn. Magn. Mater.* **121**, 490 (1993).
20. Y.-C. Chang, C.-W. Su, S.-C. Chang and Y.-H. Lee, *Eur. Phys. J. Appl. Phys.* **53**, 21501 (2011).

21. R. S. Retherford, R. Sabia and V. P. Sokira, *Appl. Surf. Sci.* **183**, 264 (2001).
22. C.-Y. Han, C.-W. Lai, Y.-F. Chao, K.-C. Leou and T.-L. Lin, *Appl. Surf. Sci.* **257**, 2536 (2011).
23. O. Y. Filatov and L. V. Poperenko, *Appl. Surf. Sci.* **253**, 163 (2006).
24. A. Larenaa, F. Millán, Gloria Pérez and G. Pinto, *Appl. Surf. Sci.* **187**, 339 (2002).
25. W. E. J. Neal, *Appl. Surf. Sci.* **2**, 445 (1979).
26. G. A. Steele, O. Dial, Spyview: 2D/3D image Analysis Software, ver. 0.1, GNU GPL license (2011).
27. C.-L. Tien, Y.-R. Lyu and S.-S. Jyu, *Appl. Surf. Sci.* **254**, 4762 (2008).
28. F. C. Chen, Y. E. Wu, C. W. Su and C. S. Shern, *Phys. Rev. B* **66**, 184417 (2002).
29. J. H. Lai, S. H. Su, H.-H. Chen, J. C. A. Huang and C.-L. Wu, *Phys. Rev. B* **82**, 155406 (2010).
30. E. Shipton, K. Chan, T. Hauet, O. Hellwig and E. E. Fullerton, *Appl. Phys. Lett.* **95**, 132509 (2009).
31. R. L. Comstock, *Introduction to Magnetism and Magnetic Recording* (Wiley, New York, 1999).